PCCP

ROYAL SOCIETY OF CHEMISTRY

PERSPECTIVE

View Article Online
View Journal | View Issue



Cite this: *Phys. Chem. Chem. Phys.*, 2024, **26**, 16931

# "Nano-egg" superstructures of hydrophobic nanocrystals dispersed in water

M. P. Pileni

Received 28th March 2024,
Accepted 18th April 2024

DOI: 10.1039/d4cp01299b

rsc.li/pccp

In this feature article, we use hydrophobic ferrite ($Fe_3O_4$) nanocrystal shells filled with Au nanocrystals self-assembled into 3D superlattices and dispersed in water. These superstructures act as nano-heaters. The stability of such superstructures is very high, even for several years, when stored at room temperature. When subjected to an electron beam, the inverted structure of $Fe_3O_4$ structures is gradually dissolved due to the formation of hydrated electrons and hydroxyl radicals.



## I. Introduction

Over the last few decades, the structural study of materials existing in mother nature shows that they are, often, self-assembled at different scales. These hierarchical design principles are ubiquitously used to maximize functionality from a limited choice of available components. Here we give a few examples related to our subject, which are very limited compared with the many that are known: a crystal has been described for over two centuries as a microscopic arrangement of atoms in a highly periodic order, characterized by its unit periodic cells stacked in 3D space to form the crystal. In 1984, D. Shechtman[1] described a newly ordered but non-periodic crystal structure. The ordered patterns never repeat in the absence of translational symmetry. These new crystals, called "quasicrystals", can have properties that normal crystals cannot. A very aggressive and hostile debate took place for many years, ignoring the fact that a meteorite[2] is characterized by quasicrystalline structures. Another example concerns opals,[3] which are micrometer-sized silica particles self-assembled into crystalline structures. The size and order of the particles determine their optical properties. Bellini[4] in 1963 discovered that various morphotypes of bacteria in water samples persistently swam northward called magnetotactic bacteria. Blakemore[5] had the advantage of electron microscopy by which he discovered that these magnetotactic bacteria possess organelles called magnetosomes. This leads to the conclusion that self-organization in colloidal suspensions leads to a fascinating range of beautiful crystal structures, revealing not only more than just a pretty face, but also new materials with collective and intrinsic properties.

*Sorbonne Université, Department of Chemistry, 4 Place Jussieu, 75005 Paris, France. E-mail: mppileni@orange.fr; Web: https://supranano.wordpress.com*

Over the past two decades, a conceptual analogy has been observed between atomic crystals and 3D superlattices of nanocrystals: atoms and atomic bonds are replaced by incompressible nanocrystals and coating agents acting like mechanical springs. Crystals with periodic arrangements[6] and quasicrystals[7] of nanocrystals were produced. These 3D superlattices display collective properties[8–11] that are mainly due either to dipolar interactions or intrinsic properties linked to the order of the nanocrystals. Most of these properties of 3D superlattices have been obtained from hydrophobic nanocrystals deposited on a substrate.[8–19]

Given the large number of applications envisaged in diverse fields such as thermal energy release, catalysis, plasmonics and biomedicine, we need to produce a new class of advanced materials based on assembled nanocrystals dispersed in an aqueous solution.

A few years ago, we reported on the design of novel water-soluble superstructures formed by the controlled assembly of nanocrystals.[20] Colloidosomes are a shell of one or more layers of hydrophobic ferrite ($Fe_3O_4$) nanocrystals with very high flexibility, deformability and low Young's modulus.[21] These colloidosomes were internalized in tumor cells with a clear increase in cellular uptake compared to the same nanocrystals coated with hydrophilic surfactants and dispersed in an aqueous solution. This increase in nanocrystal density was observed in the vicinity of the lysosome membrane. It is important to note that the nanocrystals remain assembled in the cells whereas dispersed nanocrystals aggregate randomly.[22] Instead of shells as in the case of colloidosomes, supraballs are large, solid, dense spherical assemblies in the fcc structure of $Fe_3O_4$ nanocrystals. These different superstructures, dispersed in water, are characterized by less deformation than that with colloidosomes due to the interdigitation/deformation of ligands between nanocrystals providing a spring-like response and restoring the initial structure.

In addition, the elastic modulus is also greater than that of colloidosomes, suggesting that the mobility of the nanocrystals in the supraballs is less than that in colloidosomes.[21] By subjecting supraballs or 3D superlattices of Au nanocrystals[23] dispersed in water to a laser treatment, light–heat conversion is achieved. They function as efficient nano-heaters.[24] Thus, due to the dilution of the metal phase, the penetration depth of visible light is much greater than that of homogeneous metal nanoparticles of similar size, allowing a high average thermal load throughout the assembly. In addition, the organic matrix, which is not absorbed directly, acts as an internal reservoir for efficient energy accumulation in a few hundred picoseconds. Similar behavior is observed with colloidosomes. With the latter, the efficiency of the nano-heater varies according to its environment: in an aqueous solution, due to the limited quantity of self-assembled nanocrystals in the shell, this effect is much less pronounced than with supraballs. However, in cells, the marked increase in the density of internalised self-assembled nanocrystals triggers local photothermal damage that is inaccessible to isolated nanocrystals and not predicted by global temperature measurements.[25] Such nano-heaters could represent a tremendous opportunity for the process of releasing thermal energy as well as biomedicine.

In this feature article, we present another type of superstructure called "nano-eggs": colloidosomes of $Fe_3O_4$ nanocrystals are filled with Au nanocrystals, which evolve from disordered assemblies to 3D superlattices. These superstructures are expected to combine the properties of colloidosomes and those of tightly packed Au nanocrystals, acting as efficient nano-heaters.[27] It is also shown that in an aqueous solution, these structures remain very stable in dried systems where $Fe_3O_4$ nanocrystals are dissolved in the aqueous solution when subjected to an electron beam.

## II. Results and discussion

Here, $Fe_3O_4$ nanocrystals ranging in size from 3 nm to 10 nm are coated with oleic acid and they self-assemble to form a shell, called colloidosomes (Fig. 1a). This superstructure with a size from 150 nm to 250 nm is dispersed in an aqueous solution. To produce these colloidosomes, an aqueous solution containing dodecyltrimethylammonium bromide (DTAB) is added to the colloidal solution of $Fe_3O_4$ nanocrystals dispersed in a mixture of chloroform and octadecene (ODE). The resulting emulsion is stabilized by the addition of an ethylene glycol solution containing polyvinylpyrrolidone, heated under an $N_2$ atmosphere and left under air to gradually reach room temperature. The resulting nanocrystal assemblies are washed twice with ethanol and dispersed in deionized water to form stable colloids. Thus, the hydrophobic $Fe_3O_4$ nanocrystals self-assemble to produce colloidosomes which are dispersed in the aqueous phase, thanks to DTAB acting as a coating agent of hydrophobic colloidosomes. For more information, this procedure has been described elsewhere.[26]

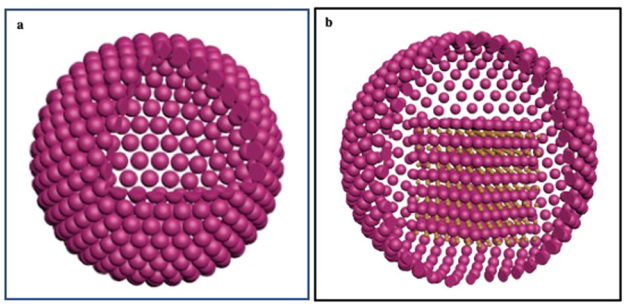


Fig. 1 Scheme of a colloidosome (a) and a nano-egg (b).

The Cryo-TEM image of these spherical colloidosomes is shown in Fig. 2a. This superstructure is very stable for more than a few years. The deposition of droplets of the colloidal solution on a coated TEM grid shows a Voronoi pattern (Fig. 2b). This shows the viscoelastic properties of such colloidal solutions, which resemble soap bubbles, mainly attributed to gas diffusion between bubbles subjected to different pressures.[28] A magnified TEM image shows deflated superstructures of $Fe_3O_4$ nanocrystals with a concave configuration (Fig. 2c). This is due to the drying process and confirms the high flexibility and elasticity of colloidosomes.[21,29] The nanocrystals retain their integrities and self-assemble into compact hexagonal network arrays or bilayers. Single or a few layer shells of $Fe_3O_4$ nanocrystals are hexagonally packed (Fig. 2d). The inner shell of the bilayer is the back part of oleic acid covalently bonded to $Fe_3O_4$ nanocrystals while the outer shell is composed of DTAB in the aqueous phase and ODE in the chloroform phase.

When spherical $Fe_3O_4$ nanocrystals are replaced by their cubic counterparts,[30] with an average edge length and distribution of 14.4 nm and 8%, highly stable colloidosomes of cubic nanocrystals, dispersed in an aqueous solution, are formed (Fig. 3a). However, deposition of this aqueous solution on a TEM grid shows that the colloidosomes tend to collapse during the drying process. This phenomenon can be attributed to the shape effect of the nanocrystal. Stronger face-to-face interactions between neighbouring nanocubes favor the formation of a planar rather than spherical organization. However, the nanocubes remain highly ordered as shown in Fig. 3b and c with specific interactions between facets. Similar results are obtained for $CoFe_2O_4$ nanocubes with similar edge lengths ($\sim$13.2 nm).

At this point, the question is whether these colloidosomes can be filled with dodecanthiol-coated Au nanocrystals to produce "nano-egg" superstructures (Fig. 1b). Note that dodecanthiol is a hydrophobic coating agent. We know that mixing two building blocks of respectively large and small sizes induces the formation of either single-component 3D superlattices or a binary crystal structure.[31,32] The type of binary crystals produced can be partially predicted from a hard sphere model[33] based on the relative sizes of the nanocrystals used. However other factors such as the relative concentration of nanocrystals and deposition temperature[34] favour the formation of single-component 3D superlattices.

Let us consider superstructures produced with 10 nm $Fe_3O_4$ and 5 nm Au nanocrystals coated with oleic acid and dodecanthiol respectively. To visualize the superstructures produced

 

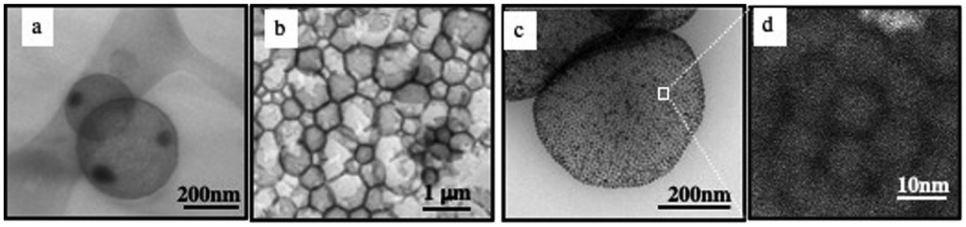


Fig. 2 (a) Cryo-TEM image of colloidosomes. (b) Low magnification TEM image of the colloidosomes after solvent evaporation (water) deposited on copper grids coated with a carbon film. (c) Magnification TEM image of a colloidosome and (d) high-magnification image of the nanocrystal assembly, shown in (c), in a hexagonal network.[20]

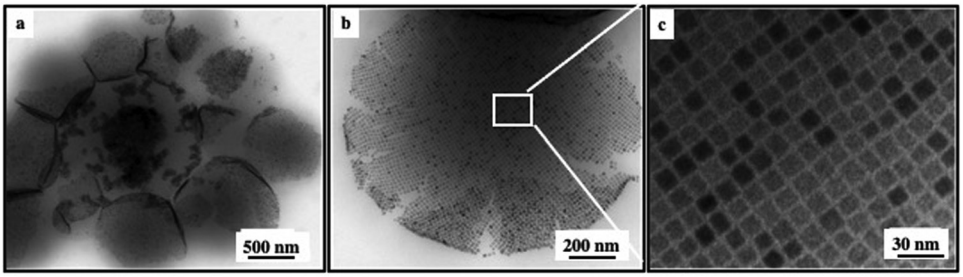


Fig. 3 TEM images of a colloidosome of $Fe_3O_4$ nanocubes at different scales.[20]

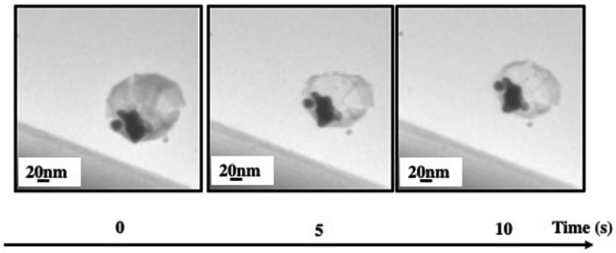


Fig. 4 "Egg" suprastructures of 4 mg $mL^{-1}$ of $Fe_3O_4$ NCs and 0.3 mg $mL^{-1}$ of Au NCs dispersed in an aqueous solution. The electron dose is around $1.69 \times 10^{+4}$ e $nm^{-2}$ $s^{-1}$.

in their native liquid medium *in situ* liquid cell transmission electron microscopy (LTEM) experiments are performed.[35–38] On a very short electron beam exposure (less than a minute), Fig. 4 shows a spherical "egg" bubble-shaped superstructure with a shell and a local aggregate with low and high contrast respectively. The difference in atomic number makes it possible to assign $Fe_3O_4$ nanocrystals to the shell and Au nanocrystals to the aggregate filled on one side of the internal cavity.

A drop of the superstructure is deposited on a TEM grid. At the end of solvent evaporation, 2D TEM images show dried superstructures (Fig. 5). At a low amount of Au nanocrystals, aggregates are observed at the edge of the $Fe_3O_4$ nanocrystal layers. They are located on one side of the inert cavity retaining a hollow interior (Fig. 5a, b and 6a, c). As the quantity of Au nanocrystals increases, Au aggregates progressively fill the hollow interior to reach Au nanocrystal assemblies surrounded by $Fe_3O_4$ nanocrystal shell(s) (Fig. 5c, d and 6e, g).

By enhancing the 2D TEM images, we observe that the Au nanocrystals progressively self-assemble into an fcc crystal

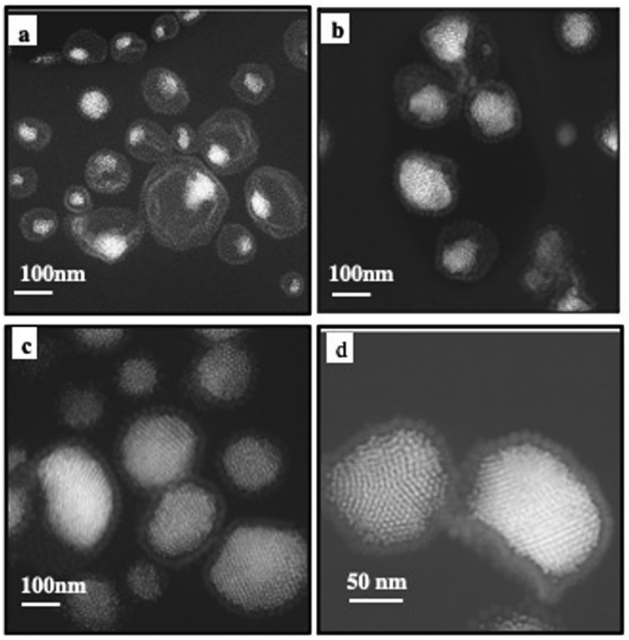


Fig. 5 2D HAADF-STEM (a)–(d) overview of superstructures of 10 nm $Fe_3O_4$ nanocrystals (2 mg $mL^{-1}$) and 5 nm Au nanocrystals differing by their amounts: (a) 10 mg $mL^{-1}$, (b) 60 mg $mL^{-1}$, (c) 100 mg $mL^{-1}$ and (d) 200 mg $mL^{-1}$.

structure (Fig. 6): at low Au nanocrystal quantities, the building blocks of the Au aggregate are partially disordered (Fig. 6b and d). As the amount of Au nanocrystals increases, the order of Au nanocrystals gradually improves (Fig. 6f) reaching local five-fold symmetry indicating that such a multi-twined structure may correspond to an icosahedral structure (Fig. 6h).

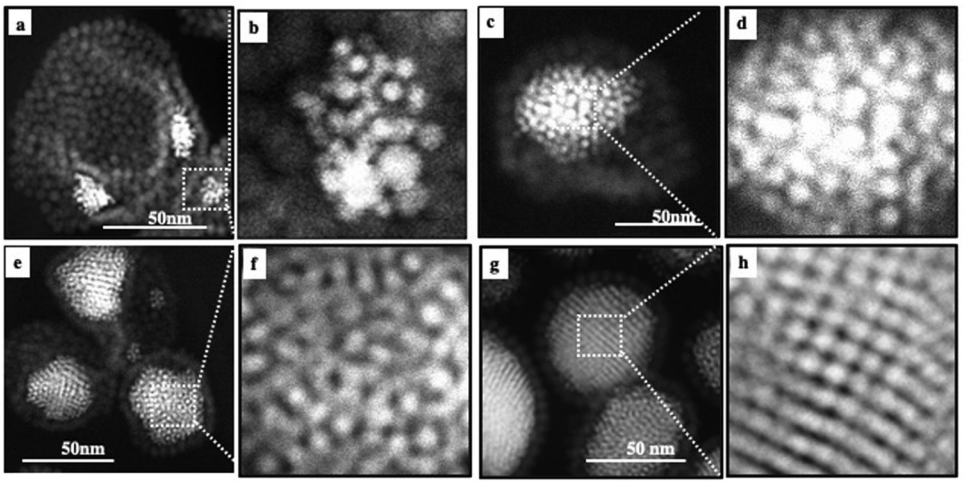


Fig. 6 High resolution 2D HAADF-STEM images (a), (c), (e) and (g) and enhancement of the nanocrystal ordering (b), (d), (f) and (h) of 10 nm $Fe_3O_4$ nanocrystals (2 mg $mL^{-1}$) and 5 nm Au nanocrystals differing by their amounts: (a) and (b) 10 mg $mL^{-1}$, (c) and (d) 60 mg $mL^{-1}$, (e) and (f) 100 mg $mL^{-1}$ and (g) and (h) 200 mg $mL^{-1}$.

Chemical mapping by energy dispersive X-ray spectroscopy (EDS) confirms the existence of one or more monolayer/multilayer shells of $Fe_3O_4$ nanocrystals. For a low percentage of Au to $Fe_3O_4$ nanocrystals, thiol-coated Au nanocrystals are located at the edge of the internal cavity. By progressively increasing the proportion of Au nanocrystals, the assemblies reach the center of the superstructures (Fig. 7).

Instead of using 10 nm $Fe_3O_4$ and 5 nm Au nanocrystals, let's perform the same experiments as described above with 6.5 nm $Fe_3O_4$ and 3.5 nm Au nanocrystals retaining the same coating agents (oleic acid and dodecanthiol respectively). Under these conditions, the hard sphere model predicts the formation of $NaZn_{13}$ or $AlB_2$-type structures.[33] Fig. 8 shows the cryo-TEM images of the colloidosomes. At the edge of the superstructure, a cubic shaped structure with brighter contrast is observed in Fig. 8a indicating the formation of an aggregate involving Au nanocrystals. The $Fe_3O_4$ nanocrystals remain in the colloidosome shell (Fig. 8b).

The HAADF-STEM images obtained after the deposition of the colloidal solution on a substrate confirm the presence of both a shell consisting of nanocrystals and a rectangular assembly inside the colloidosomes (Fig. 9a and b). The chemical analysis following STEM-EDS elemental mapping verifies the structure (Fig. 9e and f). A careful analysis of the inner assembly along the $\langle 001\rangle_{SL}$ and $\langle 011\rangle_{SL}$ zone axes (Fig. 9a–d) indicates a $NaZn_{13}$-type $(Fe_3O_4)Au_{13}$ structure similar to those deduced from the crystal model (Fig. 9g and h).[31,32] The chemical analysis following STEM-EDS elemental mapping verifies the structure (Fig. 9e and f). Due to the inherent cubic lattice of the $NaZn_{13}$ structure, anisotropic 3S superlattice

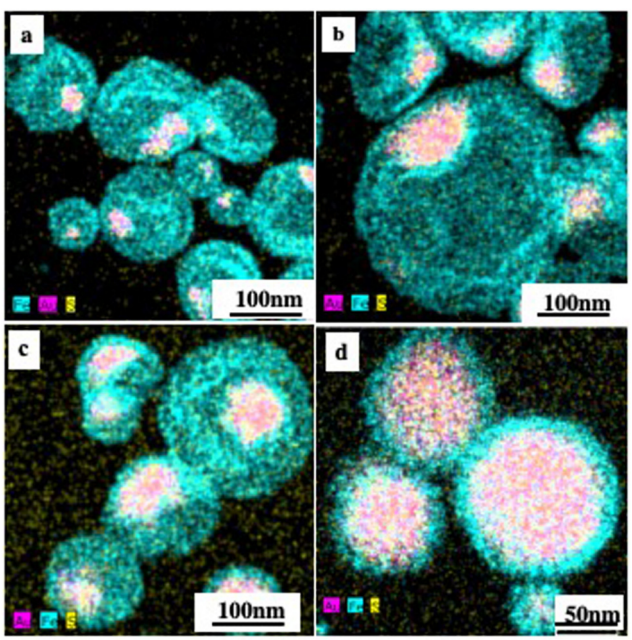


Fig. 7 EDS mapping (a)–(d) overview of "egg" superstructures of 10 nm $Fe_3O_4$ nanocrystals (2 mg $mL^{-1}$) and 5 nm Au NCs differing by their amounts such as 10 mg $mL^{-1}$ (a), 60 mg $mL^{-1}$ (b), 100 mg $mL^{-1}$ (c) and 200 mg $mL^{-1}$ (d). Cyan, magenta and yellow denote Fe, Au and S elements respectively.

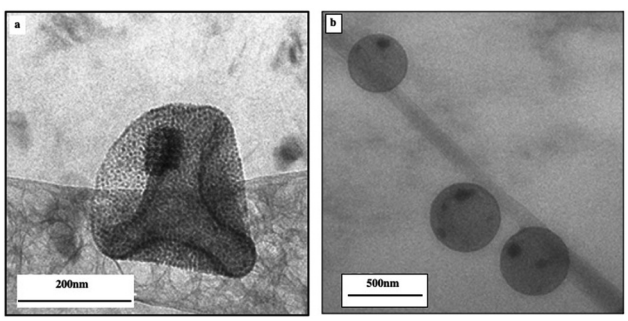


Fig. 8 Cryo-TEM image of a single colloidosome assembled from the $Fe_3O_4$/Au binary mixture.[20]

 

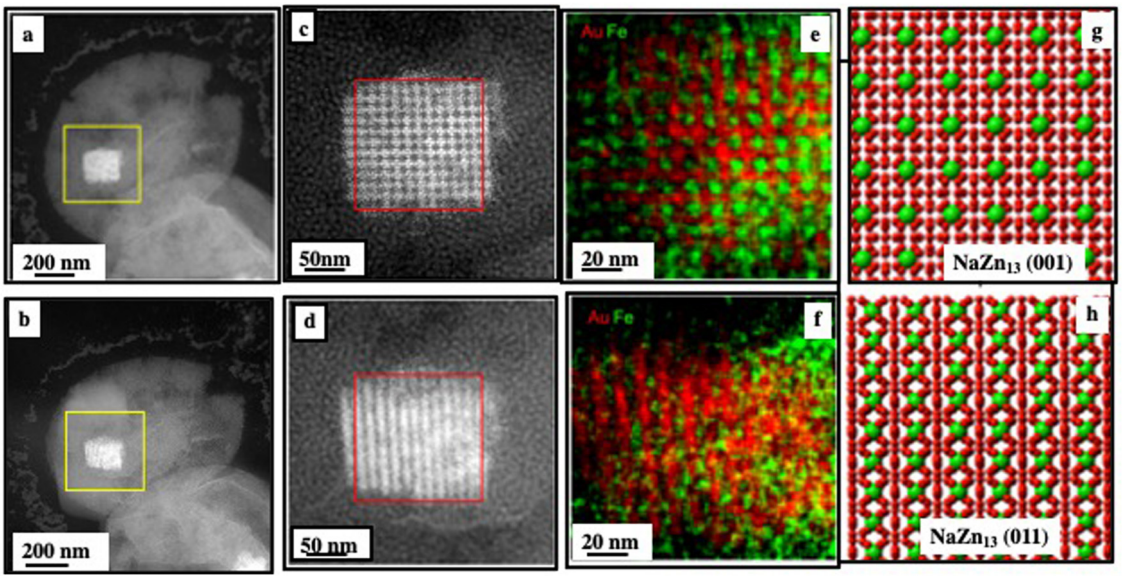


Fig. 9 HAADF-STEM images of a single colloidosome, showing the cracked structure after the drying process, tilted 45° with respect to each other (a) and (b); enlarged images (c) and (d) of the regions indicated by the yellow squares in (a) and (b) respectively; (e) and (f) STEM-EDS maps from the regions indicated by the red squares in (c) and (d) respectively; and (g) and (h) model of the $NaZn_{13}$ structure: a 45° rotation along the *x* axis leads to a transition from a ⟨001⟩ to a ⟨011⟩ zone axis.[20]

growth occurs, resulting in an anisotropic cuboid of binary 3D superlattices.

Let us consider the properties of such superstructures dispersed in an aqueous solution. The absorption spectrum of self-assembled $Fe_3O_4$ nanocrystals in colloidosomes drops markedly compared to the same nanocrystals dispersed in water and it is close to zero in the visible range. This change in the absorption spectrum of $Fe_3O_4$ nanocrystals is attributed to the fact that superstructures are metamaterials whose properties change relative to their building blocks. Indeed, addition of ethanol to the superstructures dispersed in an aqueous solution induces the destruction of these assemblies and the absorption spectrum of the dispersed nanocrystals is recovered. Conversely, the contribution of Au nanocrystals, *i.e.* localized surface plasmon resonance (LSPR), increases, as expected, with its percentage. Thus, with 10% Au relative to the $Fe_3O_4$ nanocrystals, the contribution of Au aggregates is rather small and is progressively more pronounced and slightly red shifts relative to the dispersed Au nanocrystals (Fig. 10).

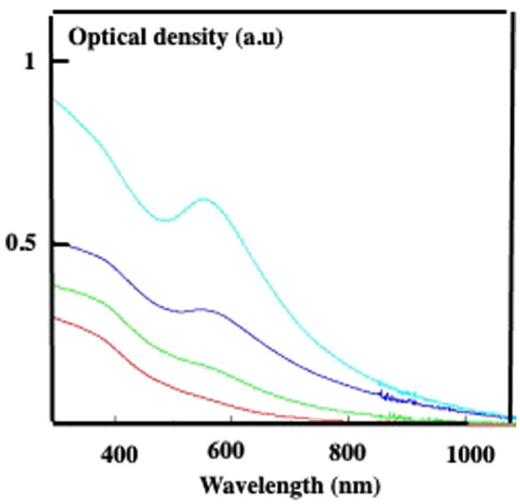


Fig. 10 Absorption of nano-eggs differing by their amount of Au nanocrystals involved in the aggregate. The percentage of Au compared to $Fe_3O_4$ is (a) 10% red, (b) 60% green, (c) 100% blue and (d) 200% light blue.

Here we study the energy flow during light irradiation, pump–probe experiments with ultrashort laser pulses.[27] A 100-fs pump pulse at 400-nm wavelength is used to excite the nano-eggs that differ in their relative amount of Au *versus* $Fe_3O_4$ nanocrystals. Fig. 11 shows the differential transmission spectra ($\Delta T/T$) recorded as a function of time, $t$, and the probe wavelength, $\lambda$. The transient optical response of plasmonic superstructures exhibits two distinct behaviors: a short-lived transient of the order of a few picoseconds is followed by a positive transient signal appearing in less than 100 ps and characterized by a very long lifetime (up to several ns). The transient signals increase in absolute value with the increase in the quantity of Au nanocrystals in the superstructures due to the larger size of the plasmonic nanocrystal assembly, without substantial distortions in the spectrum. This reveals the possibility of tailoring the photothermal properties of nano-egg superstructures by exploiting plasmonic assembly effects.

At the initial timescale of ten picoseconds, corresponding to the horizontal section of the 2D maps, the transient signal resembles the typical $\Delta T/T$ map recorded for plasmonic nanoparticles. Fig. 12 shows the measured $\Delta T/T$ for various wavelengths corresponding to colloidosomes filled with 3D superlattices of Au or $Au(Fe_30_4)_{13}$ respectively. These transients have a decay constant of a few picoseconds, dominated by the

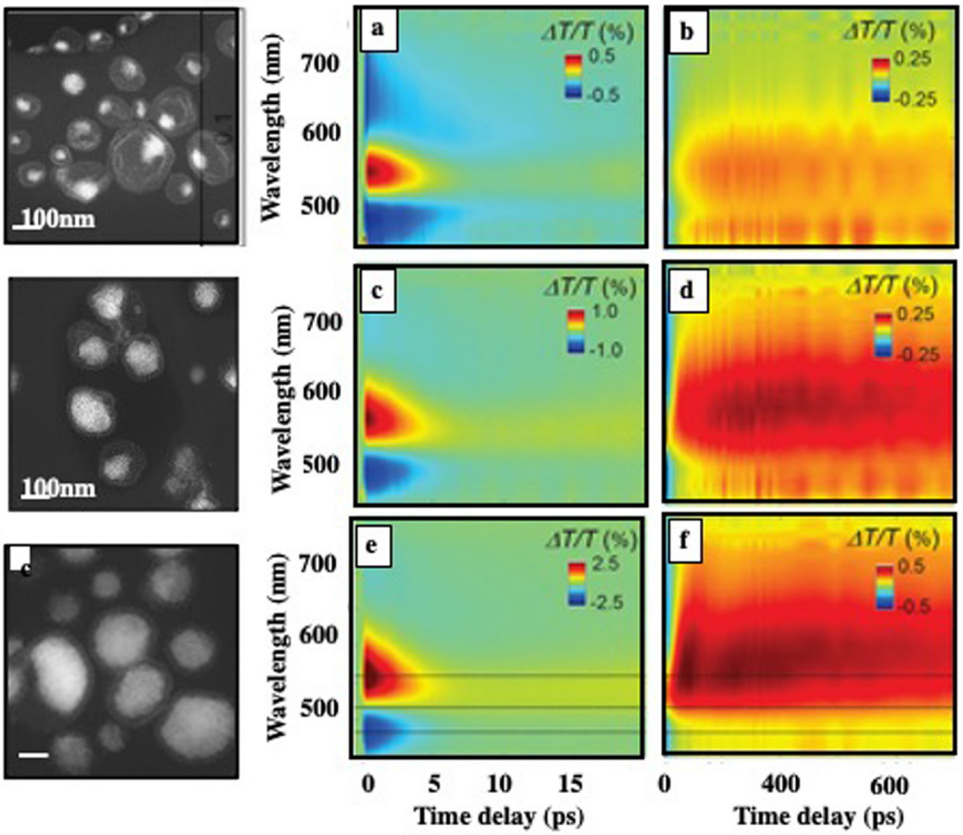


Fig. 11 Ultrafast transient differential transmittance at different wavelengths and time scales is recorded for superstructures differing in their relative amount of Au nanocrystals *versus* $Fe_3O_4$ nanocrystals. The relative percentages are (a, b) 10%, (c, d) 60% and (e, f) 100%. (a, c, e) Corresponds to the short delay (<10 ps) and (b, d, f) to the longer delay (800 ps). The pump excitation wavelength is $\lambda$ = 400 nm and the pulse fluence $F_p \sim 340$ μJ cm$^{-2}$.

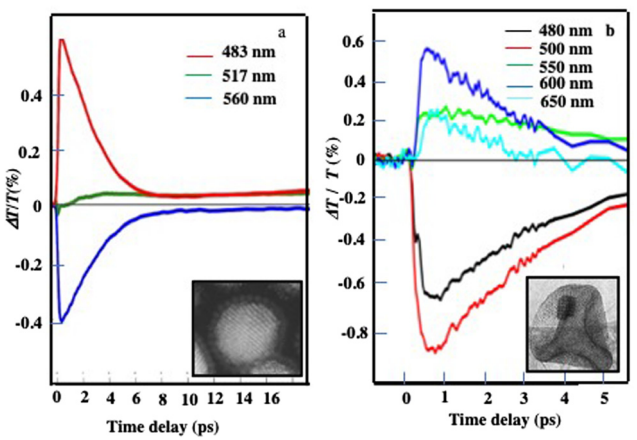


Fig. 12 Dynamics of the $\Delta T/T$ at selected probe wavelengths, at short time scales of energy flow in the (a) Au and (b) $Au(Fe_3O_4)_{13}$ superstructures.[27]

shift and broadening of plasmon resonances as observed previously.[39] They correspond to the time scale of electron–phonon scattering in noble metals.[40] Therefore, Au assemblies retain the fingerprint of their building blocks. This is attributed to the ultrafast nonlinear dynamics of the metal's internal degrees of freedom, namely the excess energy in a non-thermalized part of out-of-equilibrium carriers, an electronic temperature, and the Au lattice temperature. As a result, Au "cluster" structures at room temperature retain the fingerprint of isolated nanocrystals used as building blocks. This has also been observed, by scanning tunneling microscopy/scanning tunneling spectroscopy (STM/STS) experiments at low temperatures, with thick and dried Au 3D superlattices.[41]

At longer time scales, as observed with 3D superlattices of 5 nm Au nanocrystals dispersed in an aqueous solution,[24] the temporal dynamics, at selected probe wavelengths (Fig. 11b, d and f), show a red-shifted positive transient. The shift is around 100 nm relative to the first spectrum. The appearance of this broadband transient signal occurs within approximately 100–150 ps. Then, the transient remains constant on the nanosecond scale while a monotonic decay over time generally reaches zero above 10 ps. The signals (Fig. 13) correspond to horizontal sections of 2D maps in Fig. 11. The nanostructuring inside the core of the superstructure plays a central role in the photothermal process of heating the matrix, which is responsible for the delayed build-up of the optical signal. In fact, the behavior observed at longer times cannot be explained by the presence of the Au phase alone.

According to previous studies with Au 3D superlattices[24] dispersed in an aqueous phase, this phenomenon cannot be attributed to mechanical oscillations.[42] Indeed, after

 

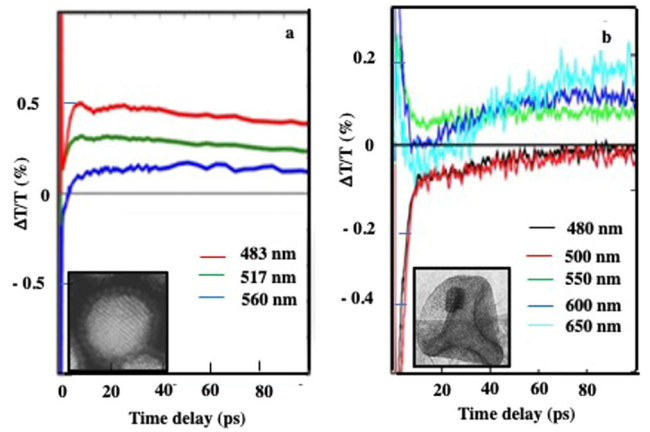


Fig. 13 Dynamics of the $\Delta T/T$ at selected probe wavelengths, at long-time scales of energy flow in the (a) Au and (b) $Au(Fe_3O_4)_{13}$ superstructures.[27]

accumulation, the signal remains constant on the nanosecond scale and bears a clear imprint of mechanical oscillations with an oscillation period of around 300 ps, attributed to an ensemble breathing mode as previously observed in dried 3D superlattices of Ag nanocrystals.[43] This unexpected transient optical response was also observed with the binary superstructures described in Fig. 8 and 9 and with supraballs.[24] This result was attributed to a much greater visible light penetration depth than that of homogeneous metal nanocrystals of similar size. This enables a high average thermal load throughout the assembly. The organic matrix, which does not absorb directly, acts as an internal reservoir for efficient energy accumulation within a few hundred picoseconds. From there, a collective regime of photo-temperature generation is made possible by the 3D superstructures dispersed in an aqueous solution. Simulations[27] were carried out to compare the characteristic energy relaxation times of dispersed and assembled Au nanocrystals. The thermal properties show substantial differences in the photothermal response, which is greatly enhanced in the presence of Au nano-assemblies. Collective effects can occur and higher temperatures are reached, allowing a more efficient heating process governing the thermo-optics observed for superstructures. This clearly shows that Au "nano-egg" superstructures behave similarly to the other superstructures dispersed in an aqueous solution and act as nano-heaters.

Similar pump–probe experiments were carried out with 5 nm Au nanocrystals coated with dodecanthiol, used as building blocks for 3D superlattices. When 3D hydrophobic Au superlattices are dispersed in an aqueous solution by intertwining the alkyl chains of the Au nanocrystals with lipid vesicles, short- and long-lifetime transients are observed as described above.[23,24] In contrast, with the same Au 3D superlattices deposited on a substrate (dried assemblies), only the short time transient is observed.[44] Similarly, with hydrophobic Co nanocrystals self-assembled into 3D superlattices and deposited on a substrate, only the short-lifetime transient is observed.[45] This clearly indicates that this unexpected long lifetime signal has to be related to the presence of water. To propose an explanation for such a new positive long lifetime signal, first, let's take a look at how these superstructures were made: Au 3D superlattices are first fabricated in a-polar solvents and then coated with biological molecules, enabling them to be dispersed in water. During the manufacture of the "nano-egg" superstructures, the reagents are all in contact with water. Note that $Fe_3O_4$ and Au nanocrystals are coated with oleic acid and dodecanthiol respectively. When these hydrophobic coating agents are subjected to contact water molecules, some of them tend to adsorb and bind to alkyl chains, as observed with carbon nanotubes in the presence of water.[46] For first approximation, we can assume that water molecules are confined within the superstructures *via* their organic surfactant molecules. As with carbon nanotubes, exotic properties of water confined within 3D superlattices could emerge. This could be an eternal debate, given the difficulties of understanding the action of water in many fields. However, we propose a hypothesis: we know that this positive signal is attributed to the coating agents acting as an internal reservoir for efficient energy accumulation. This process could be facilitated by an increase in flexibility and/or a decrease in the viscosity of surfactant molecules induced by the presence of water molecules in the network. Indeed, as in liquid crystals,[47] which have long-range ordered structures, it could be assumed that in superstructures where the "local" concentrations of surfactants are very high, there would be a significant level of free and bound water molecules. As such, they would enable a reduction in viscosity and/or greater flexibility of alkyl chains.[48] This, in turn, activates the energy transfer and accumulation in the organic matrix.

Our aim here is to examine the stability of this nano-egg superstructure. In the absence of external phenomena such as temperature, light, and electron beam, these superstructures are stable for several years. Light does not appear to be a significant parameter for disrupting the stability of such superstructures. Let's look at the influence of the electron beam. The water-dispersed superstructures are placed in a liquid cell transmission electron microscope (LTEM) in a manner similar to what is shown in Fig. 3. To achieve a better resolution of the superstructures compared to what was presented above, the thickness of the cell is reduced. Fig. 14 shows that by increasing the exposure time to the electron beam, a progressive dissolution of the $Fe_3O_4$ nanocrystalline structure leading to a total disappearance is observed while Au remains present. It should be noted that fusion of Au nanocrystals could occur. The technique is not sensitive enough to confirm such a hypothesis.

To confirm such behavior, we subjected colloidosomes dispersed in an aqueous solution or deposited on a substrate to an electron beam for similar exposure times. In an aqueous solution, by increasing the exposure time to the electron beam, a progressive dissolution of the $Fe_3O_4$ nanocrystals leading to their total disappearance and consequently to the superstructures is observed as shown in Fig. 15a–d. Conversely, when the same colloidosomes are deposited on the TEM grid, the superstructures retain their structures (Fig. 15e–h). This clearly indicates that water plays a major role in the stability of $Fe_3O_4$ nanocrystals and should be attributed to the formation

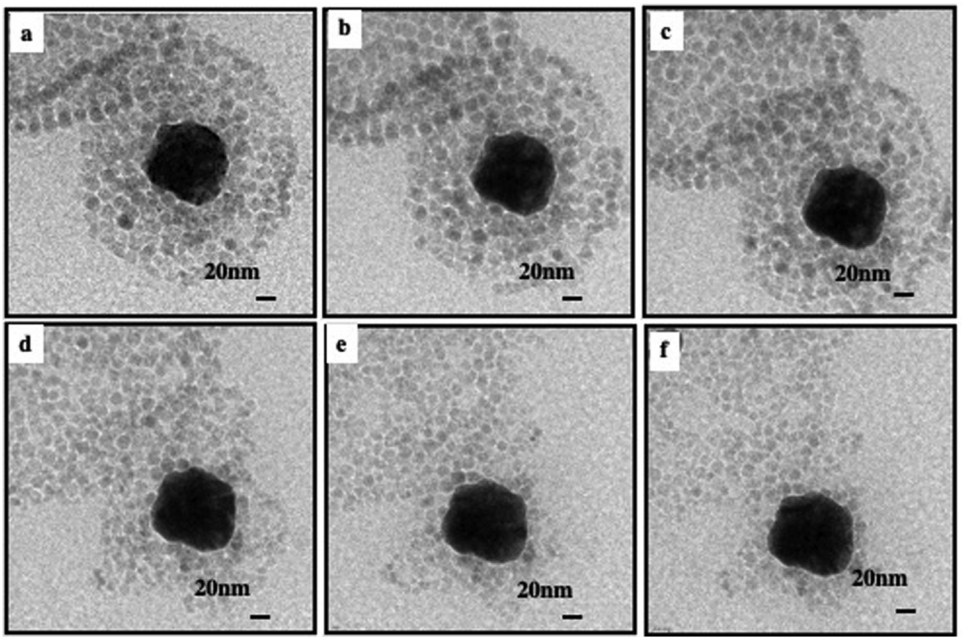


Fig. 14 Evolution with time of a "nano-egg" superstructure (4 mg $mL^{-1}$ and 0.3 mg $mL^{-1}$ of 10 nm $Fe_3O_4$ and 5 nm Au nanocrystals respectively) subjected to various times of electron beam exposure. The electron dose is around $1.69 \times 10^{+4}$ e $nm^{-2}$ $s^{-1}$. Exposure time (a) $t$ = 0; (b) $t$ = 1.5 min, (c) $t$ = 5 min, (d) $t$ = 9 min, (e) 11 min and (f) $t$ = 12 min.

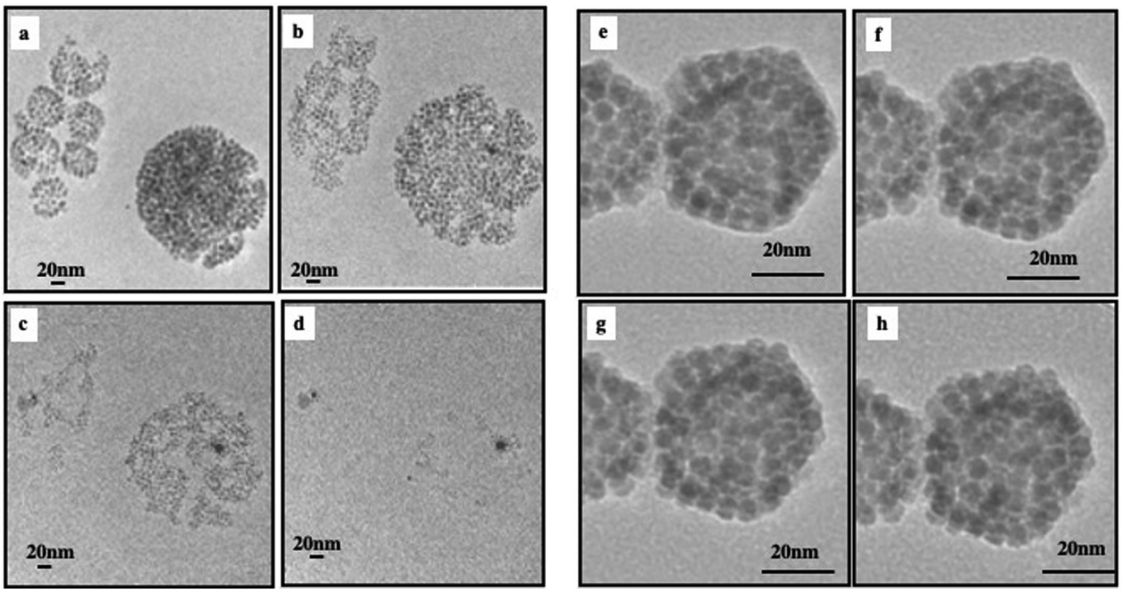


Fig. 15 Evolution with time of colloidosome superstructures (4 mg $mL^{-1}$ of 10 nm $Fe_3O_4$ nanocrystals) dispersed in an aqueous solution (a)–(d) and deposited on a substrate (e)–(h). They are subjected to various times of electron beam exposure. The electron dose is around $1.69 \times 10^{+4}$ e $nm^{-2}$ $s^{-1}$. Exposure time (a) and (e) $t$ = 0; (b) and (f) $t$ = 5 min, (c) and (g) $t$ = 10 min, (d) and (h) $t$ = 12 min.

of hydrated electrons and hydroxyl radicals in the presence of water when the colloidal solution is subjected to electron beam.

To explain such dissolution of $Fe_3O_4$ nanocrystals subjected to an electron beam, we need to consider the crystal structure of $Fe_3O_4$: it is an inverse spinel whose unit cell consists of 32 oxygen ions ($O^{2-}$) in a face-centered cubic structure. $Fe^{2+}$ and half of $Fe^{3+}$ occupy octahedral sites and the other half of $Fe^{3+}$ occupies tetrahedral sites. Under the electron beam, the hydrated electron ($e^-_{aq}$) and the hydroxyl radical ($OH^\bullet$) are the main species produced. Highly reactive hydroxyl radicals attack most organic molecules and can easily oxidize oxygen ions. This process breaks the order of the oxygen ions in their fcc network. At the same time, $Fe^{2+}$ and $Fe^{3+}$ ions can be partially reduced by the hydrated electrons and oxidized by

 

the OH radicals. The action of the hydroxyl radicals and the hydrated electrons breaks the crystalline structure and induces the dissolution of $Fe_3O_4$ nanocrystals. In the absence of hydroxyl radicals and hydrated electrons, *i.e.* in a dried system, both hydrated electrons and hydroxyl radicals are not produced and hence the crystalline structure remains intact. This result is essential, as one of the problems associated with the use of nanocrystals in biomedicine is that they accumulate in the liver, kidneys and lymphatic system. Although $Fe_3O_4$ nanocrystals are highly effective materials, this accumulation poses a huge constraint to their use in patient care. The fact that $Fe_3O_4$ nanocrystals can be dissolved by subjecting them to an electron beam opens up the real potential for their use in biomedicine.

With ''nano egg'' superstructures we have no information regarding practical applications. However, with colloidosomes we have demonstrated that such superstructures exhibit an increase in cellular uptake by tumor cells compared to the same nanocrystals used as building blocks, coated with a hydrophilic agent and consequently dispersed in an aqueous solution. Moreover, an increase in the nanocrystal density close to the lysosome membrane takes place. Importantly, nanocrystals remain assembled in cells whereas dispersed nanocrystals are randomly aggregated.[22] On subjecting the internalized colloidosomes to a magnetic field, they align and form long chains. According to the fact that nanocrystal self-assemblies in aqueous environments behave as universal nano-heaters, these self-assemblies trigger local photothermal damage inaccessible to isolated nanocrystals and not predicted by global temperature measurements.[25]

## III. Conclusion

In this feature article, we present ''nano-egg'' superstructures dispersed in an aqueous solution: hydrophobic $Fe_3O_4$ nanocrystals self-assembled to produce a shell composed of one and/or more layers, called colloidosomes, are filled with aggregates of Au nanocrystals evolving from disordered assemblies to 3D superlattices. These ''nano-egg'' superstructures act as nano-heaters while other assemblies[49] dispersed in an aqueous solution, attributed to a high average thermal load throughout the assembly with organic surfactant molecules, act as an internal reservoir for efficient energy accumulation. Taking into account the data presented here and in other studies, we have concluded that when hydrophobic nanocrystals are self-assembled into 3D superlattices and dispersed in an aqueous solution, they become good candidates for energy storage, solar energy and biomedicine applications. It should be mentioned that dispersion of the assemblies in water is mandatory to create nano-heaters. Indeed, with dried assemblies, the excess energy could be released into the substrate and is not transferred to the organic alkyl chains. This could be due to the hydration effect of the alkyl chains when water is present in the medium. In an aqueous solution, $Fe_3O_4$ nanocrystals dispersed in water are dissolved, whereas they are not in dried systems when subjected to an electron beam. This opens up a major opportunity for the use of these nanocrystals in biomedicine. One of the major problems in all these biomedical applications is the accumulation of $Fe_3O_4$ nanocrystals in the liver, lungs, and kidneys. This dissolution should make it possible to use $Fe_3O_4$ nanocrystals for a large number of applications, particularly in biomedicine.

According to the data presented here and in other studies, water is a major factor in the use of superstructures such as nano-heaters. These unexcepted data need to be elucidated. It is clear that energy transfer could be facilitated by increasing the flexibility of organic alkyl chains. In addition, we need to examine the internalization process of these nano-eggs, as we did with colloidosomes. We might expect an increase in the effectiveness of hyperthermia in cell death. The future will teach us the future of such superstructures.

## Conflicts of interest

No conflicts of interest.

## Acknowledgements

My special thanks to Profs. S. Balls, G. Cerullo, G. de La Vallée, G. Rizza, D. Yang, and Z. Yang.

## References

1 D. Shechtman, I. Blech, D. Gratias and J. W. Chan, Metallic Phase with Long-Range Orientational Order and No Translational Symmetry, *Phys. Rev. Lett.*, 1984, **53**, 1951.
2 S. Glotzer, Quasicrystals: the thrill of the chase, *Nature*, 2019, **565**, 156.
3 J. V. Sanders, Color opal, *Nature*, 1964, **204**, 1151–1153.
4 S. Bellini, Su di un particolare comportamento di batteri d'acqua dolce (On a unique behavior of freshwater bacteria), Institute of Microbiology, University of Pavia, Italy, 1963.
5 R. P. Blakemore, Magnetotactic bacteria, *Science*, 1975, **190**, 377–379.
6 A. Courty, J. Richardi, P. A. Albouy and M. P. Pileni, How to control the crystalline structure of supracrystals of 5-nm Ag nanocrystals, *Chem Mat.*, 2011, **23**, 4186–4192.
7 Z. Yang, J. Wei, P. Bonville and M.-P. Pileni, Beyond Entropy: Magnetic Forces Induce Formation of Quasicrystalline Structure in Binary Nanocrystal Superlattices, *J. Am. Chem. Soc.*, 2015, **137**, 4487–4493.
8 M. P. Pileni, Nanocrystals self-assemblies: fabrication and collective properties, *J. Phys. Chem.*, 2001, **105**, 3358–3372.
9 M.-P. Pileni, Supracrystals of Inorganic Nanocrystals: An Open Challenge for New Physical Properties, *Acc. Chem. Res.*, 2008, **41**, 1799–1809.
10 M. P. Pileni, Supra and Nano crystallinity: Specific properties related to crystal growth mechanisms and nanocrystallinity, *Acc. Chem. Res.*, 2012, **45**, 1965–1972.

11 M. P. Pileni, Impact of the metallic crystalline structure on the properties of nanocrystals and their mesoscopic assemblies, *Acc. Chem. Res.*, 2017, **50**, 1946–1955.
12 A. Zabet-Khosousi and A. Dhirani, Charge transport in nanoparticle assemblies, *Chem. Rev.*, 2008, **108**, 4072–4124.
13 M. A. Boles, M. Engel and D. V. Talapin, Self-assembly of colloidal nanocrystals: From intricate structures to functional materials, *Chem. Rev.*, 2016, **116**, 11220–11289.
14 R. Das, N. Rinaldi-Montes, J. Alonso, Z. Amghouz, E. Garaio, J. A. Garcia, P. Gorria, J. A. Blanco, M. H. Phan and H. Srikanth, Boosted Hyperthermia Therapy by Combined AC Magnetic and Photothermal Exposures in Ag/$Fe_3O_4$ Nanoflowers, *ACS Appl. Mater. Interfaces*, 2016, **8**, 25162–25169.
15 S. Alizadeh and Z. Nazari, A Review on Gold Nanoparticles Aggregation and Its Applications, *J. Chem. Rev.*, 2020, **2**, 228–242.
16 L. Zhang, Q. Fan, X. Sha, P. Zhong, J. Zhang, Y. Yin and C. Gao, Self-assembly of noble metal nanoparticles into sub-100 nm colloidosomes with collective optical and catalytic properties, *Chem. Sci.*, 2017, **8**, 6103–6110.
17 L. Motte, F. Billoudet and M.-P. Pileni, Self-Assembled Monolayer of Nanosized Particles Differing by Their Sizes, *J. Phys. Chem.*, 1995, **99**, 16425–16429.
18 N. L. Rosi and C. A. Mirkin, Nanostructures in biodiagnostics, *Chem. Rev.*, 2005, **105**, 1547–1562.
19 Y. Hui, X. Yi, F. Hou, D. Wibowo, F. Zhang, D. Zhao, H. Gao and C. X. Zhao, Understanding the Effects of Nanocapsular Mechanical Property on Passive and Active Tumor Targeting, *ACS Nano*, 2019, **13**, 7410.
20 Z. Yang, T. Altantzis, D. Zanaga, S. Bals, G. Van Tendeloo and M.-P. Pileni, Supracrystalline Colloidal Eggs: Epitaxial Growth and Freestanding Three-Dimensional Supracrystals in Nanoscaled Colloidosomes, *J. Am. Chem. Soc.*, 2016, **138**, 3493–3500.
21 I. Dobryden, Z. Yang, P. M. Claesson and M.-P. Pileni, Water Dispersive Suprastructures: an Organizational Impact on Nanomechanical Properties, *Adv. Mater. Interfaces*, 2021, **8**, 2001687.
22 A. Nicolas-Boluda, Z. Yang, T. Guilbert, L. Fouassier, F. Carn, F. Gazeau and M.-P. Pileni, Self-Assemblies of $Fe_3O_4$ Nanocrystals: Toward Nanoscale Precision of Photothermal Effects in the Tumor Microenvironment, *Adv. Funct. Mater.*, 2020, **31**, 2006824.
23 N. Yang, C. Deeb, J. L. Pelouard, N. Felidj and M. P. Pileni, Water-Dispersed Hydrophobic Au Nanocrystal Assemblies with a Plasmon Fingerprint, *ACS Nano*, 2017, **11**, 7797–7806.
24 A. Mazzanti, Z. Yang, M. G. Silva, N. Yang, G. Rizza, P.-E. Coulon, C. Manzoni, A. M. de Paula, G. Cerullo, G. Della Valle and M.-P. Pileni, Light-Heat Conversion Dynamics in Highly Diversified Water-Dispersed Hydrophobic Nanocrystal Assemblies, *Proc. Natl. Acad. Sci. U. S. A.*, 2019, **116**, 8161–8166.
25 A. Nicolas-Boluda, Z. Yang, T. Guilbern, L. Fouassier, F. Carn, F. Gazeau and M. P. Pileni, Self-Assemblies of $Fe_3O_4$ nanocrystals: Toward nanoscale precision of photothermal effects in the tumor microenvironment, *Adv. Funct. Mater.*, 2020, (1–17), 2006824.
26 D. Yang, Z. Yang, G. Rizza, S. Balls and M. P. Pileni, personal communication.
27 A. Schirato, L. Moretti, Z. Yang, A. Mazzanti, G. Cerullo, M. P. Pileni, M. Maiuri and G. Della Valle, Chemically-Controlled Ultrafast Photothermal Response in Plasmonic Nanostructured Assemblies, *J. Phys. Chem. C*, 2022, **126**(14), 6308–6317.
28 K. E. Mueggenburg, X.-M. Lin, R. H. Goldsmith and H. M. Jaeger, Elastic membranes of close-packed nanoparticle arrays, *Nat. Mater.*, 2007, **6**, 656–660.
29 A. D. Dinsmore, M. F. Hsu, M. G. Nikolaides, M. Marquez, A. R. Bausch and D. A. Weitz, Colloidosomes: Selectively Permeable Capsules Composed of Colloidal Particles, *Science*, 2002, **298**, 1006.
30 M. I. Bodnarchuk, M. V. Kovalenko, H. Groiss, R. Resel, M. Reissner, G. Hesser, R. T. Lechner, W. Steiner, F. Schaeffler and W. Heiss, Exchange-Coupled Bimagnetic Wüstite/Metal Ferrite Core/Shell Nanocrystals: Size, Shape, and Compositional Control, *Small*, 2009, **5**, 2247–2252.
31 J. Cheon, J. I. Park, J. S. Choi, Y. W. Jun, S. Kim, M. G. Kim, Y. M. Kim and Y. J. Kim, *Proc. Natl. Acad. Sci. U. S. A.*, 2006, **103**, 3023–3027.
32 E. V. Shevchenko, D. V. Talapin, S. O'Brien and C. B. Murray, Polymorphism in AB13 Nanoparticle Superlattices: An Example of Semiconductor−Metal Metamaterials, *J. Am. Chem. Soc.*, 2005, **127**, 8741–8747.
33 M. D. Eldridge and P. A. Madden, Frenkel, Entropy-driven formation of a superlattice in a hard-sphere binary mixture D, *Nature*, 1993, **365**, 35–37.
34 Z. Yang, J. Wei and M.-P. Pileni, Metal−Metal Binary Nanoparticle Superlattices: A Case Study of Mixing Co and Ag Nanoparticles, *Chem. Mater.*, 2015, **27**, 2152–2157.
35 N. de Jonge and F. M. Ross, Electron Microscopy of Specimens in Liquid, *Nat. Nanotechnol.*, 2011, **6**, 695–704.
36 F. M. Ross, Opportunities and Challenges in Liquid Cell Electron Microscopy, *Science*, 2015, **350**(6267), AAA9886.
37 N. Hodnik, G. Dehm and K. J. J. Mayrhofer, Importance and Challenges of Electrochemical *in situ* Liquid Cell ElectronMicroscopy for Energy Conversion Research, *Acc. Chem. Res.*, 2016, **49**, 2015–2022.
38 S. Pu, C. Gong and A. W. Robertson, Liquid cell transmission electron microscopy and its application, *R. Soc. Open Sci.*, 2020, **7**(1–24), 191204.
39 M. G. Silva, D. C. Teles-Ferreira, L. Siman, C. R. Chaves, L. O. Ladeira, S. Longhi, G. Cerullo, C. Manzoni, A. M. de Paula and G. Della Valle, Universal saturation behavior in the transient optical response of plasmonic structures, *Phys. Rev. B*, 2018, **98**, 115407.
40 C. Sun, F. Vallée, L. H. Acioli, E. P. Ippen and J. G. Fujimoto, Femtosecond-tunable measurement of electron thermalization in gold, *Phys. Rev. B: Condens. Matter Mater. Phys.*, 1994, **50**, 15337–15348.
41 P. Yang, I. Arfaoui, T. Cren, N. Goubet and M. P. Pileni, Unexpected Electronic Properties of Micrometer-Thick

 

Supracrystals of Au Nanocrystals, *Nano Lett.*, 2012, **12**, 2051–2055.
42 G. V. Hartland, Optical Studies of Dynamics in Noble Metal Nanostructures, *Chem. Rev.*, 2011, **111**, 3858–3887, PMID: 21434614.
43 A. Courty, A. Mermet, P. A. Albouy, E. Duval and M. P. Pileni, Self-organized Ag-nanocrystals in fcc ''supra'' crystals: Vibrational Coherence, *Nat. Mater.*, 2005, **4**, 395–398.
44 N. Goubet, I. Tempra, J. Yang, G. Soavi, D. Polli, G. Cerullo and M. P. Pileni, Size and nanocrystallinity controlled gold nanocrystals: synthesis, electronic and mechanical properties, *Nanoscale*, 2015, **7**, 3237–3246.
45 I. Lisiecki, D. Polli, C. Yan, G. Soavi, E. Duval, G. Cerullo and M. P. Pileni, Coherent Longitudinal Acoustic Phonons in Three-Dimensional Supracrystals of Cobalt Nanocrystals, *Nano Lett.*, 2013, **13**, 4914–4919.
46 A. Chatzichristos and J. Hassan, Current Understanding of Water Properties inside Carbon Nanotubes, *Nanomaterials*, 2022, **12**, 174.
47 G. Tiddy, The properties of water in concentrated surfactant and colloid systems, *J. Taiwan Inst. Chem. Eng.*, 2018, **92**, 20–28.
48 C. P. Baryiames, P. Garrett and C. R. Baiz, Bursting the bubble: A molecular understanding of surfactant-water interfaces, *J. Chem. Phys.*, 2021, **154**, 170901.
49 M. P. Pileni, Superstructures of water-dispersive hydrophobic nanocrystals: specific properties, *Mater. Horiz.*, 2023, **10**, 4746.